Increased ratio of rapsyn to ACh receptor stabilizes postsynaptic receptors at the mouse neuromuscular synapse

Othon L. Gervásio and William D. Phillips

Department of Physiology, Institute for Biomedical Research, The University of Sydney, NSW 2006 Australia

The metabolic turnover of nicotinic ACh receptors (AChR) at the neuromuscular synapse is regulated over a tenfold range by innervation status, muscle electrical activity and neural agrin, but the downstream effector of such changes has not been defined. The AChR-associated protein rapsyn is essential for forming AChR clusters during development. Here, rapsyn was tagged with enhanced green fluorescent protein (EGFP) to begin to probe its influence at the adult synapse. In C2 myotubes, rapsyn–EGFP participated with AChR in agrin-induced AChR cluster formation. When electroporated into the tibialis anterior muscle of young adult mice, rapsyn–EGFP accumulated in discrete subcellular structures, many of which colocalized with Golgi markers, consistent with the idea that rapsyn assembles with AChR in the exocytic pathway. Rapsyn–EGFP also targeted directly to the postsynaptic membrane where it occupied previously vacant rapsyn binding sites, thereby increasing the rapsyn to AChR ratio. At endplates displaying rapsyn–EGFP, the metabolic turnover of AChR (labelled with rhodamine-α-bungarotoxin) was slowed. Thus, the metabolic half-life of receptors at the synapse may be modulated by local changes in the subsynaptic ratio of rapsyn to AChR.

(Received 19 October 2004; accepted after revision 17 November 2004; first published online 25 November 2004)
Corresponding author W. D. Phillips: Department of Physiology (F13), Institute for Biomedical Research, The University of Sydney, NSW 2006 Australia. Email: billp@physiol.usyd.edu.au

Formation of the postsynaptic cluster of acetylcholine receptors (AChR) at the neuromuscular synapse is initiated by neural agrin, which activates MuSK (muscle-specific kinase; Gautam *et al.* 1996; Glass *et al.* 1996). Rapsyn, a third essential component, binds the cytoplasmic face of the AChR and recruits new receptors to a scaffold formed by MuSK (Gautam *et al.* 1995; Apel *et al.* 1997). Rapsyn facilitates linkage of AChRs to the detergent-resistant cytoskeleton through a process that involves activation of src and fyn kinases (Mohamed & Swope, 1999; Mittaud *et al.* 2001; Mohamed *et al.* 2001). A number of upstream signal transduction pathways and protein–protein interactions are likely to be involved (Sanes & Lichtman, 2001; Bezakova & Ruegg, 2003; Godfrey & Schwarte, 2003; Megeath *et al.* 2003).

The precise nature of the complex formed between AChR and rapsyn remains to be fully defined (Ramarao *et al.* 2001). Since rapsyn is capable of interacting with each one of the five subunits of the AChR, the assembled, pentameric AChR might contain as many as five rapsyn-binding sites (Huebsch & Maimone, 2003). However, studies with the postsynaptic membrane of Torpedo electric organ suggest that only one or two molecules of rapsyn attach to each AChR channel (Burden *et al.* 1983; LaRochelle & Froehner, 1986; Miyazawa *et al.* 1999). Studies in cell culture and Torpedo electric organ indicate that at least some rapsyn associates with newly formed AChR during its trafficking from the Golgi apparatus to the plasma membrane (Marchand *et al.* 2002). Importantly, treatment of myotubes with neural agrin increased the amount of rapsyn immunoprecipitated per AChR during the process of AChR clustering (Moransard *et al.* 2003). Thus the ratio of rapsyn to AChR increases at the time of synapse formation.

In spite of extensive studies of AChR cluster formation in cell culture and knockout mice, the precise role of rapsyn at the mature neuromuscular synapse remains to be determined. A key issue at the mature synapse is the metabolic half-life ($t_{1/2}$) of the AChR. Turnover of AChR within the postsynaptic membrane is regulated over a wide range. During embryonic development and in cultured muscle cells, AChRs are metabolized rapidly ($t_{1/2} = 12$–24 h), being internalized and proteolysed (Reiness & Weinberg, 1981). The half-life of synaptic AChR increases to about $t_{1/2} = 10$–13 days postnatally in rat (Reiness & Weinberg, 1981). Muscle electrical activity helps maintain the long half-life of synaptic AChRs (Andreose *et al.* 1993; Akaaboune *et al.* 1999). Similarly,

 DOI: 10.1113/jphysiol.2004.077685

overexpression of neural agrin can stabilize AChRs that are clustered in denervated adult muscle (Bezakova *et al.* 2001). Finally, half-life may be influenced by the tightness with which AChRs are tethered within the postsynaptic membrane, since lateral diffusion into the neighbouring perisynaptic membrane makes AChR vulnerable to endocytosis (Akaaboune *et al.* 1999; Akaaboune *et al.* 2002; Grady *et al.* 2003). Here we present evidence that rapsyn can target to the adult postsynaptic AChR cluster at variable ratios of rapsyn to AChR. Higher rapsyn to AChR ratios slowed AChR turnover.

Methods

Expression plasmids and immunoblotting

Mouse rapsyn cDNA was fused upstream of jellyfish enhanced green fluorescent protein (EGFP) in pEGFP-N1 (Clontech, Palo Alto, CA, USA). The rapsyn–EGFP chimera was confirmed by sequencing. QT-6 fibroblasts were transfected as previously described (Phillips *et al.* 1997). Whole-cell lysates were immunoblotted with antirapsyn monoclonal antibody (mAb)1234 (Froehner, 1984) using ECL-Plus chemiluminescence as described (Amersham, UK; Liang *et al.* 2001). Expression plasmid encoding α-2,6-sialyltransferase tagged with a VSV-G epitope (Rabouille *et al.* 1995) was a gift from Dr Rob Parton (Institute for Molecular Bioscience, St Lucia, QLD, Australia).

Electroporation of muscle fibres

Sterile expression plasmids purified by Qiagen Maxiprep (Qiagen, UK) were introduced into muscle fibres of living mice by electroporation (Mir *et al.* 1999). Five-week-old female FVB mice were anaesthetized with 5 μl g^{-1} I.P. of a mixture of ketamine and xylazine in sterile isotonic saline (final concentration 1 mg ml^{-1} ketamine; 10 mg ml^{-1} xylazine; Troy Laboratories, Australia). The tibialis anterior (TA) muscle was surgically exposed. Ten micrograms of plasmid DNA in 10 μl of sterile MilliQ water (Millipore Corp., Billerica, Massachusetts, USA), was layered over the muscle surface (Lee *et al.* 2002). Silver electrodes were placed on either side of the muscle, touching the surface of the DNA solution but not the muscle. Six monopolar square-wave pulses were applied perpendicular to the long axis of the muscle (duration 50 ms, field strength 200 V cm^{-1} at 1 Hz; Mir *et al.* 1999). Electroporation was followed by suture and subcutaneous injection of Temgesic (30 μl buprenorphine (300 μg ml^{-1}); Reckitt Benckiser, Australia). Following recovery on a warming pad, mice became active within about 1 h and were observed regularly. At time of kill, mice were anaesthetized as above, followed by cervical dislocation. This project was approved by the Animal Ethics Committee of The University of Sydney.

FRAP and fluorescence microscopy

Fluorescence recovery after photobleaching (FRAP) results shown in Fig. 1 involved C2 myotubes transfected with rapsyn–EGFP. C2 myoblasts were transfected with rapsyn–EGFP expression plasmid using Lipofectamine-Plus (Invitrogen, Carlsbad, CA, USA). Myotubes formed from these myoblasts were treated overnight with a soluble C-terminal neural agrin preparation as described (Han *et al.* 1999). Coverslips with myotubes attached were bathed in Dulbecco's modified Eagle's medium (DMEM) without phenol red (Invitrogen), and labelled with tetramethylrhodamine isothiocyanate-α-bungarotoxin (TRITC-α-BGT; Molecular Probes, Eugene, OR, USA; 5 ng μl^{-1} final concentration in DMEM with no phenol red, 1 h at 37°C). After washing with DMEM, cells were imaged with a ×63 NA 1.2 water-immersion objective by laser scanning microscopy (Leica DM IRE2 inverted microscope equipped with a Leica TCS SP2 system, Germany) at room temperature (RT). The number of large AChR clusters was determined by examining every adjacent microscope field on the GFP channel. Transfected myotubes were classified as to whether they displayed diffuse cytosolic rapsyn–EGFP (high-level expressers) or not (low-level expressers). A myotube segment was that portion of a myotube that spanned the ×63 field. AChR clusters longer than 10 μm (measured along the long axis of the myotube) were counted as large AChR clusters. Photobleach of a single spot was achieved by increasing laser power to maximum so as to bleach both TRITC and EGFP simultaneously. Recovery over time was monitored by scanning the whole field regularly at low laser power. Control myotubes were imaged to confirm that the staining represented specific fluorophor (TRITC-α-BGT or rapsyn–EGFP) rather than fluorescent cross-bleed (Han *et al.* 1999). Recently, it has been shown that very intense laser illumination can un-bind fluorescently conjugated-α-BGT from a fraction of labelled AChRs (Akaaboune *et al.* 2002). We do not think that photo-unbinding followed by re-binding of free fluorescent ligand contributed significantly to our fluorescence recovery curves for TRITC-α-BGT or rapsyn–EGFP. Little or no recovery of fluorescence was observed when the photobleach was applied to AChR clusters or in paraformaldehyde fixed cells (Figs 1 and 3).

For the FRAP experiments shown in Fig. 3, muscles were layered over with DMEM without phenol red (Invitrogen) and imaged *in situ* at RT. Imaging was performed using a Nikon Eclipse E600FN upright microscope with ×63 water-immersion objective (NA 1.0; Nikon Co., Japan) coupled to a cooled CCD camera and its associated acquisition software (RT Spot 9.0 Monochrome 6; Diagnostic Instruments, Sterling Heights, MI, USA). The excitation/emission filter set was specific for

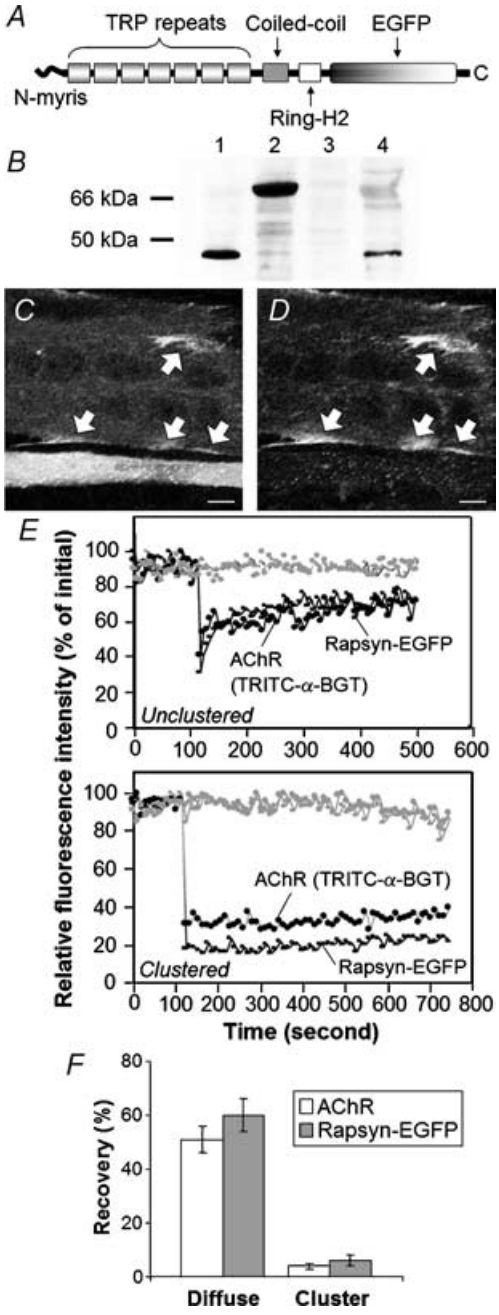

Figure 1. Fluorescence recovery after photobleaching (FRAP) analysis of rapsyn–EGFP and ACh receptors (AChRs) in C2 myotubes

A, enhanced green fluorescent protein (EGFP) was fused in-frame to the C-terminus of rapsyn: myristoylated N-terminus (N-myris), seven tetratrichopeptide (TRP) repeats, AChR-binding coiled-coil, dystroglycan-binding RING-H2 domain and enhanced green fluorescent protein (EGFP). *B*, immunoblotting revealed the expected bands when QT-6 fibroblasts were transfected with wild-type rapsyn (lane 1, ∼46 kDa), or rapsyn–EGFP (lane 2, ∼72 kDa). Endogenous (wild-type) rapsyn was also detected in C2 myotubes (lane 4). No such band was detected in nontransfected QT-6 cells (lane 3). *C* and *D*, C2 myotubes expressing transfected rapsyn–EGFP were treated with neural agrin overnight then labelled for cell surface AChRs by addition of TRITC-α-BGT to the culture medium. *C*, EGFP fluorescence channel – a large diameter myotube running horizontally across the top of the field reveals large rapsyn–EGFP-patches at the cell periphery (arrows). A thin myotube beside it, towards the bottom of the field, displays diffuse rapsyn–EGFP filling the cytosol. *D*, the TRITC-α-BGT channel showed that the large rapsyn–EGFP patches corresponded to AChR clusters (arrows). The thinner myotube (overexpressing rapsyn–EGFP) displayed only tiny AChR microaggregates. *E*, FRAP recovery curves. Fluorescent intensities for TRITC-α-BGT and rapsyn–EGFP were normalized to their values at time zero. A single spot was bleached at maximum laser power at the 100 s time point, and recovery of fluorescence intensity was recorded over time (using low-intensity scanning). TRITC-α-BGT-labelled AChRs and rapsyn–EGFP recovered with a similar time course and to a similar degree (Unclustered). Similar bleaching of a spot within an AChR cluster yielded little FRAP recovery (Clustered). Grey plots represent fluorescence intensity in a nonbleached area on the same myotube. *F*, percentage recovery of fluorescence 5 min after the photobleach event. Bars in *F* represent the mean ± S.E.M. for 10 FRAP experiments of the type shown in *E*. *C* and *D*, scale bar, 10 μm.

GFP/FITC (XF100-2; Omega Optical, Brattleboro, VT, USA). All the settings were kept constant during the imaging and analysis of the endplates. For each of the experimental conditions that are plotted together, the images were all taken in the same imaging session. The gain was set at the maximum possible without producing saturation (pixels with grey level of 255) at the beginning of each session and was not changed. A portion of the endplate (or fluorescent extrasynaptic region) was bleached by shutting down the excitation iris diaphragm and applying maximum fluorescence intensity until fluorescence was diminished to ∼1/5 of the surrounding region. As a control, the same experiment was performed on QT-6 fibroblasts transfected with rapsyn–EGFP. Fixed samples (both muscle fibres and QT-6) were used as negative controls.

For the experiments shown in Fig. 5, AChRs were labelled with TRITC-α-BGT (10 ng μl^{-1} final concentration) for 15 min at RT. This labelling protocol was sufficient to essentially saturate α-BGT binding sites at the endplate, since it inhibited subsequent labelling of the same endplates with fluoresceine-isothiocyanate-conjugated α-bungarotoxin by 98.2%. Muscle fibres were imaged using the Nikon microscope, objective, camera and acquisition software described above (filter set for TRITC: XF101-2; Omega Optical).

Immunohistochemistry and confocal microscopy

Transverse cryosections (12 μm) of electroporated muscle fibres were preincubated with 1% bovine serum albumin (Sigma) in PBS (pH 7.4) for 1 h at RT. Sections were then incubated overnight at 4°C with either anti-VSV-G (1:300; Sigma), anti-GM130 (1:100), antip115 (1:100; BD Biosciences, San Jose, CA, USA), or antirapsyn antibodies mAb1234 or mAb1579 (Froehner, 1984). Antirapsyn antibodies were used at concentrations in excess of that required for maximal endplate immunofluorescence (hybridoma supernatants diluted 1:2). After

washing three times with PBS, sections were incubated with Alexa Fluor-555-conjugated secondary antibody (1:1000; Molecular Probes) for 1 h at RT. Cryosections and cells were analysed by confocal laser scanning microscopy, as described previously. The argon (488 nm) and He/Ne (543 nm) laser lines were used for excitation of EGFP and TRITC/Alexa Fluor 555, respectively. Emission light was collected in the range of 505–530 (EGFP) and 560–600 (TRITC/Alexa Fluor 555). Final images were the result of four Kalman averages. Control sections were incubated with secondary antibody and TRITC-α-BGT (no primary antibody) to confirm the absence of significant nonspecific binding or fluorescence cross-bleed. The confocal aperture was set to 1.0 AU (Airy unit). The laser power was set as low as possible to avoid undesirable photobleaching without compromising the quality of the images (15 and 50% of power for 488 and 543 laser lines, respectively). All the settings (aperture, gain and laser power) were determined at the beginning of the imaging session, and these parameters were not changed.

Loss of TRITC-α-BGT-labelled AChR from the endplate

Retention and loss of AChR from the postsynaptic AChR cluster was studied in 5-week-old postnatal mice by labelling endplate AChRs with TRITC-α-BGT. Four days after electroporation of the TA muscle with rapsyn–EGFP, mice were again anaesthetized. The surface of the TA muscle was surgically exposed and labelled with TRITC-α-BGT (30 ng μl^{-1} in PBS) for 40 min so as to saturate AChRs at the endplate. The muscle was then washed three times with sterile PBS to remove excess TRITC-α-BGT. After suturing and recovery, mice were monitored for 4 days, and then killed. The TA muscle was then dissected and frozen for cryosectioning (experimental day 8 mice). Control mice were killed and TA muscles frozen for cryosectioning immediately after labelling with TRITC-α-BGT (day 4 mice). Day 4 and day 8 muscles were processed and imaged together under identical conditions. Sister cryosections from the same day 8 muscles were re-exposed to TRITC-α-BGT to label any newly added AChRs at the endplate. For the experiments shown in Fig. 9, the TA muscle was exposed and endplates were imaged *en face* as shown in Fig. 9*A*–*D* for residual AChR. The muscle surface was then re-incubated with TRITC-α-BGT, and the same endplates were imaged again to reveal total AChR (residual plus new added AChR). Residual and newly added AChR were expressed as a percentage of total TRITC-α-BGT for the endplate in question.

Image analysis

ImageTool 2.03 software (The University of Texas Health Science Center in Santo Antonio TX, USA; http://ddsdx.uthscsa.edu/dig/itdesc.html) was used for quantification of fluorescence intensity and area. In all quantifications, background fluorescence of surrounding rapsyn–EGFP-negative cells was measured and subtracted from the regions of interest (background fluorescence was always between 10 and 15% of absolute fluorescence). In order to confirm the linearity of the response of the CCD camera, serial dilutions of FITC- or TRITC-conjugated antibodies were spotted on a glass slide and imaged. The fluorescence intensity and concentration of the antibody were plotted in a graph and defined a straight line ($R^2 = 0.999$ for FITC; $R^2 = 0.994$ for TRITC). ImageJ 1.31v software (National Institutes of Health, Bethesda, Maryland, USA; http://rsb.info.nih.gov/ij/) was used for correlation and colocalization analysis. Imaging of rapsyn–EGFP-positive endplates and corresponding TRITC-α-BGT staining was followed by fluorescence quantification of each pixel using both images. The pixel intensity for each X,Y coordinate was plotted as a scatter plot (TRITC-α-BGT as abscissa, and rapsyn–EGFP as ordinate). Colocalization analysis was used to compare puncta of rapsyn–EGFP with the Golgi markers (sialyltransferase-VSV-G, GM130 or p115). Threshold was set in order to isolate puncta of either rapsyn–EGFP or Golgi labelling in a binary image to match the size and distribution of structures perceived by eye in the original grey scale image. Each pair of binary images (rapsyn–EGFP *versus* Golgi marker) was then overlaid. In order to assess the percentage of colocalization, regions in the overlaid binary image (positive colocalized areas) were counted and compared to the binary rapsyn or Golgi marker images.

The relationship between the brightness of two fluorophors (rapsyn–EGFP and TRITC-α-BGT) was determined by Pearson's correlation (R^2 coefficient of determination). Student's t test was used to compare means of two different groups. Results in Fig. 8 were analysed using 2-way analysis of variance with rapsyn–EGFP and time as independent variables. Mean and standard error of the mean (S.E.M.) are shown in the plots for each group.

Results

Rapsyn–EGFP targeting in cultured myotubes

EFGP was fused to the C-terminus of mouse rapsyn (rapsyn–EGFP; Fig. 1*A*). Immunoblotting of QT-6 fibroblasts transfected with rapsyn or rapsyn–EGFP expression plasmids yielded bands of the expected sizes (wild-type rapsyn ~46 kDa; rapsyn–EGFP ~72 kDa; Fig. 1*B*). Rapsyn–EGFP was then transiently transfected into the mouse muscle cell line C2. Myotubes were treated overnight with neural agrin, cell-surface AChRs were labelled with TRITC-α-BGT, and live myotubes were imaged by laser scanning microscopy. As previously

Table 1. AChR clusters on C2 myotubes expressing transfected rapsyn–EGFP

	Expression level	
	Low*	High†
Large AChR clusters/myotube segment‡	5.0	1.0
Large rapsyn–EGFP clusters/myotube segment‡	2.9	0.27
Number of segments with microaggregates§	1	20
Number of myotube segments examined	98	51

AChR, nicotinic ACh receptors; EFGP, enhanced green fluorescent protein. *Myotubes with low-level expression were those that displayed rapsyn-EGFP membrane labelling without diffuse cytosolic rapsyn-EGFP (Han *et al.* 1999). †High-level expression was defined as myotubes that displayed diffuse rapsyn–EGFP fluorescence visibly filling the cytosol. ‡Average number of AChR clusters/rapsyn–EGFP clusters that were longer than 10 μm per myotube segment (see Methods). When present, large rapsyn–EGFP clusters were always precisely colocalized with AChR clusters. §Number of myotube segments that displayed multiple AChR–rapsyn microaggregates (AChR clusters <2 μm long).

found for wild-type rapsyn, some myotubes expressed rapsyn–EGFP at such high levels that it filled the cytosol. These myotubes responded poorly to agrin, producing few large AChR clusters (Fig. 1*C*, bottom of field; Table 1; Han *et al.* 1999). Other myotubes expressed rapsyn–EGFP at lower levels (no visible diffuse cytoplasmic labelling). Such myotubes formed many large AChR clusters, at which rapsyn–EGFP accumulated (arrows in Fig. 1*C* and *D*; Table 1). Thus, as for wild-type rapsyn (Han *et al.* 1999), when expressed at low levels in myotubes, rapsyn–EGFP participated in the formation of large AChR clusters.

FRAP was then used to compare the lateral mobility of AChR within the myotube membrane with that of rapsyn–EGFP. Previous FRAP studies using TRITC-α-BGT to label AChRs showed that a large fraction of the AChR that was dispersed within the plane of the myotube plasma membrane was mobile, but that AChR became immobile when clustered (Dubinsky *et al.* 1989). In myotubes that had not been treated with neural agrin, fluorescence for TRITC-α-BGT and rapsyn–EGFP was coextensive throughout the plasma membrane (myotubes displaying diffuse cytosolic rapsyn–EGFP were excluded from these experiments for reasons outlined above). When a spot was bleached for both fluorophors, fluorescence of both recovered rapidly (Fig. 1*E*, unclustered). For nine such recovery experiments the average time to half-maximal recovery for AChR and rapsyn–EGFP was not significantly different (1.36 ± 0.48 *versus* 1.0 ± 0.21 min, respectively, $P > 0.9$). The two fluorophors also displayed a similar percentage recovery in the 5 min following photobleach (Fig. 1*F*). AChR and rapsyn–EGFP that were coclustered on agrin-treated myotubes were relatively immobile. Neither TRITC-α-BGT nor rapsyn–EGFP fluorescence recovered significantly in the 5 min monitoring period following the bleach event (Fig. 1*E*, clustered; Fig. 1*F*). The similarity of time course, extent of fluorescence recovery and the lack of recovery once clustered are consistent with the idea that AChR and rapsyn–EGFP molecules exist as a stable protein complex both prior to and following clustering.

Targeting of rapsyn–EGFP in adult muscle fibres

Rapsyn–EGFP expression plasmid was introduced into fibres of the TA muscle of 5-week-old mice by electroporation while mice were under general anaesthesia. The surface of the muscle was imaged 5 days later. A subset of muscle fibres displayed rapsyn–EGFP labelling of their endplates (Fig. 2*A*, arrowhead; Figs 5*A* and *B*). In those fibres that displayed rapsyn–EGFP-positive endplates, a region of the fibre also showed multiple puncta of rapsyn–EGFP fluorescence (Fig. 2*A*, arrows point to individual puncta). This region ($\sim$500 μm long) could be anywhere along the length of the fibre with no obvious spatial relationship to the endplate. Presumably this was where the plasmid entered the fibre at the time of electroporation. Optical sectioning revealed two different populations of rapsyn–EGFP puncta within such regions. A peripheral shell of puncta was prominent close under the sarcolemma. These peripheral puncta were approximately circular with a fairly uniform diameter of 1.31 ± 0.18 μm ($n = 637$; Fig. 2*B* and *D*). The second population of rapsyn–EGFP-labelled structures lay deeper within core of the fibre and were of more irregular shape (Fig. 2*C*). Muscle fibres on the surface of the intact muscle were analysed by FRAP to gauge the mobility of rapsyn–EGFP within the endplate, and among extra-synaptic puncta. As a control, we examined the mobility of rapsyn–EGFP expressed in the quail fibroblast cell line QT-6 under identical conditions. Transfected QT-6 cells displayed both large and small patches of rapsyn–EGFP at their periphery, as previously reported for wild-type rapsyn (Phillips *et al.* 1991). When we photobleached a portion of a large rapsyn–EGFP patch on the QT-6 cell, about 30% of the fluorescence within the bleached area recovered over a period of about 20 min (time to half-maximal fluorescence recovery 3.9 ± 1.3 min; Fig. 3*A* (QT-6); Fig. 3*B*). Fixed QT-6 cells showed no such recovery (Fig. 3*B*). The same procedure was then applied to muscle fibres on the surface of the TA muscle that displayed rapsyn–EGFP. When a portion of a rapsyn–EGFP-decorated endplate was photobleached, no recovery of fluorescence was observed over 20 min (Fig. 3*A* (Endplate); Fig. 3*B*). This suggests that rapsyn–EGFP was relatively immobile within the endplate AChR cluster, as previously found for AChR clusters on C2 myotubes (Fig. 1). This is consistent with the idea that rapsyn forms a stable interaction with clustered AChR, which is also immobile in short-term

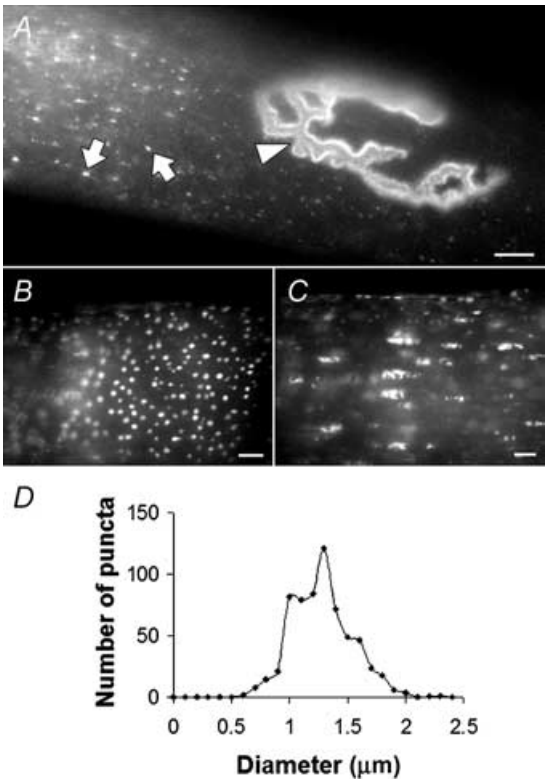

Figure 2. Subcellular targeting of rapsyn–EGFP in adult muscle fibres
Fibres of the TA muscle were imaged 5 days after electroporation with rapsyn–EGFP. *A*, rapsyn–EGFP was evident as puncta in the cytoplasm (arrows) and concentrated at endplates (arrowhead). *B* and *C*, extrasynaptic puncta of rapsyn–EGFP were found both at the periphery of the muscle fibre (*B*) and deep in the sarcoplasm (*C*). *D*, frequency distribution showing the diameter of peripheral rapsyn–EGFP puncta (1.31 ± 0.18 μm; $n = 637$). Scale bar, 10 μm.

experiments such as this (Dubinsky *et al.* 1989; Akaaboune *et al.* 2002). Similarly, when FRAP was applied to a portion of the extrasynaptic rapsyn–EGFP puncta, no recovery of fluorescence was recorded among the bleached puncta (Fig. 3*B*). The lack of measurable mobility between bleached puncta and neighbouring un-bleached puncta is consistent with the idea that the individual puncta were discrete (discontinuous) membrane compartments.

Extra-synaptic rapsyn–EGFP structures partially colocalize with Golgi markers

The size and distribution of the extrasynaptic rapsyn-EGFP-labelled puncta (Fig. 2*B–D*) were reminiscent of the distribution of the Golgi apparatus in muscle fibres (Ralston *et al.* 2001). Thus, transverse cryosections of electroporated muscle were immunolabelled with antibodies directed against the Golgi-associated proteins, α-2,6-sialyltransferase (*trans*-Golgi network (TGN resident); Chege & Pfeffer, 1990), GM130 (*cis*-Golgi) and p115 (vesicle tubular structures; Barr & Short, 2003). Rapsyn–EGFP puncta were colocalized with puncta of GM130 (Fig. 4*A–D*), sialyltransferase (Fig. 4*E–H*) and p115 (not shown), in many, but not all, cases. About half of the Golgi marker-positive structures were colocalized with rapsyn–EGFP puncta (Fig. 4*I*). Similarly, about one-third and one-half of rapsyn–EGFP puncta were colocalized with bright spots of GM130 and sialyltransferase staining, respectively (Fig. 4*J*). These results are consistent with the idea that rapsyn–EGFP targets to the Golgi apparatus and/or some closely associated structure within the adult muscle fibre.

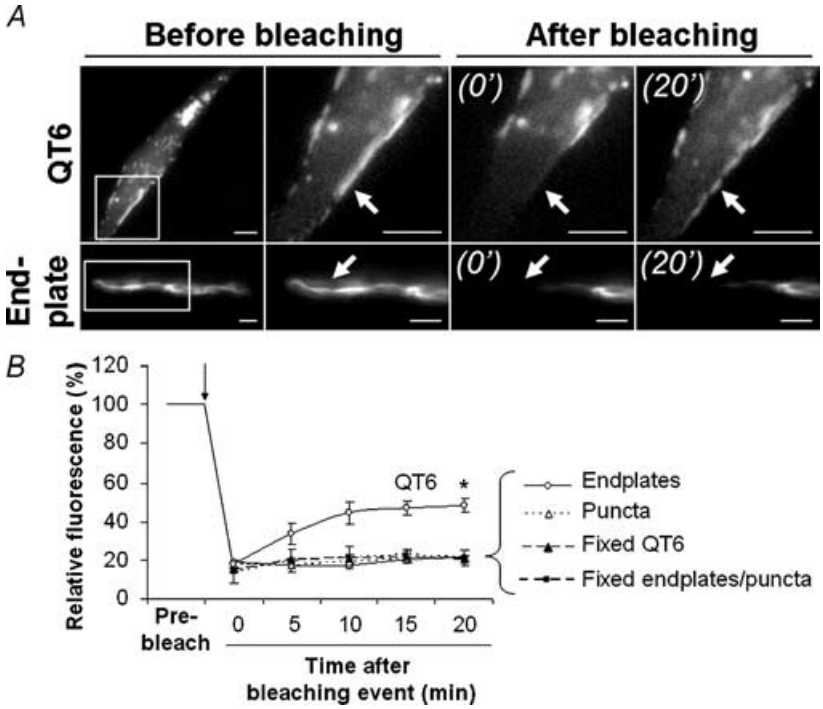

Figure 3. Rapsyn–EGFP was relatively immobile in adult muscle fibres
QT-6 fibroblasts and tibialis anterior (TA) muscle fibres transfected with rapsyn–EGFP were used for FRAP experiments. *A*, rapsyn–EGFP fluorescent images of a peripheral patch on a QT-6 cell (top row) and an endplate (bottom row) before and after photobleaching. Panels to the right show an expanded view of the boxed area before the photobleach event, then 0 min and 20 min after photobleach. *B*, FRAP recovery curves. Pixel intensities for rapsyn–EGFP within the bleached area were normalized to the intensity prior to photobleach. Peripheral patches of rapsyn–EGFP on QT-6 cells showed a 30% recovery of fluorescence over the 20 min, while endplate AChR clusters and extrasynaptic puncta showed no measurable recovery over the same period. No recovery was seen in cells or tissues fixed with 2% paraformaldehyde. *B*, data represent the mean ± S.E.M. for the minimum of nine FRAP experiments for each group (*$P < 0.001$). Scale bars: QT-6, 5 μm; endplate, 10 μm.

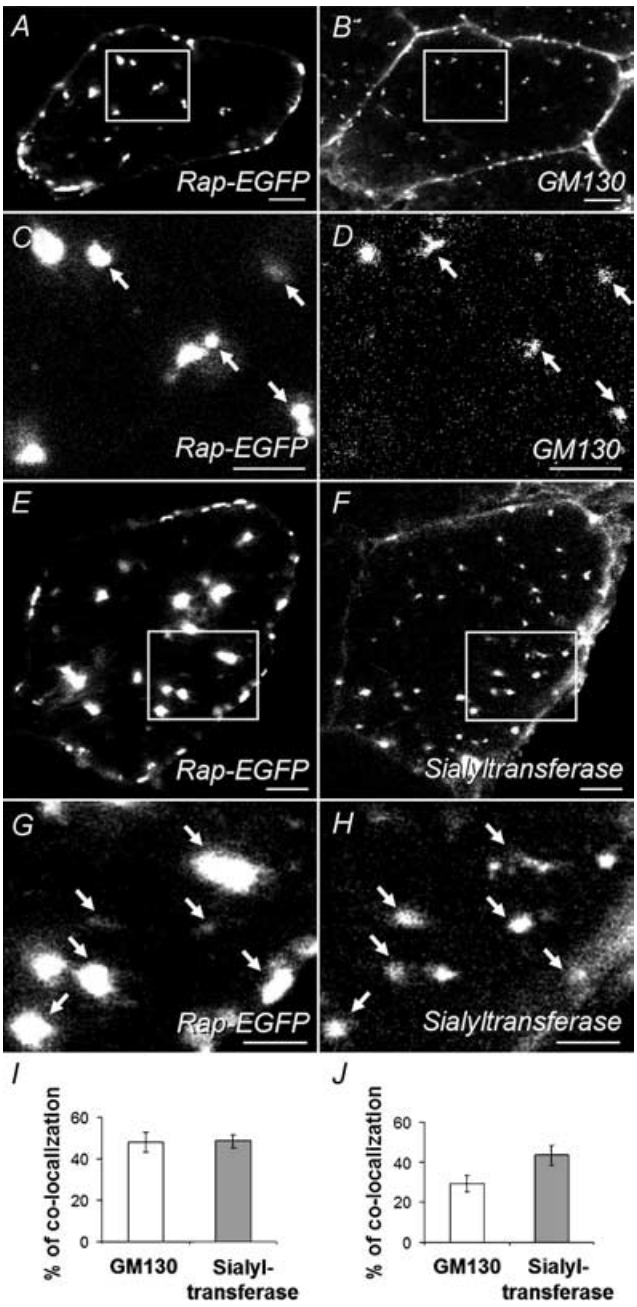

Figure 4. Extrasynaptic rapsyn–EGFP puncta partially colocalized with Golgi markers
Transverse cryosections through muscle fibres were immunofluorescently labelled with antibodies against Golgi markers followed by Alexa-Fluor-555-conjugated secondary antibody. Left-hand panels show rapsyn–EGFP fluorescence, while right-hand panels show the corresponding anti-Golgi marker fluorescence channel. *A–D*, anti-GM130 staining (*C* and *D* are enlargements of the boxed areas in *A* and *B*). *E–H*, staining for cotransfected sialyltransferase-VSV-G (*G* and *H* are enlargements of boxed areas in *E* and *F*). Many of the rapsyn–EGFP puncta were colocalized with intracellular puncta of these two Golgi markers. The antimouse secondary antibodies also directly stained the plasma membranes of all the (mouse) muscle fibres, both transfected and nontransfected (*B*, *F* and *H*). This represents nonspecific staining. However, the intracellular puncta were only seen in sections where secondary antibody was preceded by incubation with the primary Golgi-marker antibodies. *I*, the percentage of Golgi puncta (either GM130 or sialyltransferase) colocalized with rapsyn–EGFP. *J*, the percentage of rapsyn–EGFP puncta colocalized with one or other Golgi marker. Data in *I* and *J* represent the mean ± S.E.M. for 12 muscle-fibre profiles (6 for each Golgi marker) as described in Methods. Scale bars: *A*, *B*, *E* and *F*, 10 μm; *C*, *D*, *G* and *H*, 5 μm.

Rapsyn–EGFP at endplates was distributed in proportion to AChR density

In most fibres that displayed the extrasynaptic rapsyn–EGFP puncta described above, the endplate was also decorated with rapsyn–EGFP. Double labelling with TRITC-α-BGT confirmed targeting of rapsyn–EGFP to endplates (Fig. 5*A* and *B*). In contrast, free EGFP (not fused to rapsyn) showed no tendency to accumulate in puncta or at endplates. Instead, it diffusely filled the cytoplasm (Fig. 5*C* and *D*). Thus the endplate localization of rapsyn–EGFP was due to targeting of the rapsyn part of the chimera rather than the EGFP moiety. To quantitatively compare the spatial relationship of rapsyn–EGFP to AChR within the postsynaptic AChR cluster, the TRITC and EGFP pixel intensity values for individual pixels were plotted against each other. This showed a direct relationship (Fig. 5*I*). A total of 107 endplates were individually analysed in this way by scatter plot, representing 1, 2, 3, 4, 5 and 11 days after electroporation. In all cases Pearson's correlation had an R^2 coefficient greater than 0.85 ($P < 0.01$). Control images excluded the possibility of fluorescence cross-bleed between optical channels (Fig. 5*E–I*). The close quantitative spatial correlation within each endplate strongly argues that rapsyn–EGFP binds either to the AChR itself or to some molecular structure that codistributes within the postsynaptic AChR cluster in strict proportion to the AChR.

Rapsyn–EGFP can target directly to the postsynaptic AChR cluster

Rapsyn–EGFP might have accumulated at the endplate by first assembling with newly synthesized AChR within the Golgi apparatus so as to replace pre-existing AChR–rapsyn complex in the AChR cluster. If so, we would expect a progressive accumulation of rapsyn–EGFP that would complement the turnover of old AChR from the endplate ($t_{1/2} \approx 10$ days, see Discussion). Rapsyn–EGFP-positive endplates could be observed from day 1 after electroporation (the earliest time examined). The number of such endplates per TA muscle increased progressively through to at least day 11, at a rate of about three to four new rapsyn-EGFP-positive endplates per day (Fig. 6*A*), indicating ongoing synthesis of rapsyn–EGFP. The brightness of rapsyn–EGFP fluorescence at each such

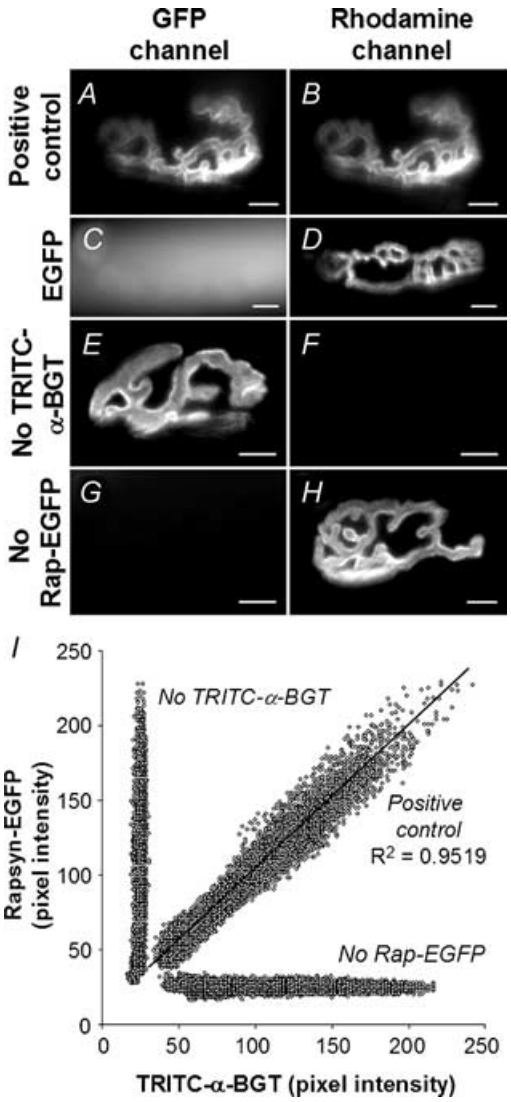

Figure 5. The spatial distribution of rapsyn–EGFP and TRITC-α-BGT-labelled AChRs was closely correlated
A–H, imaging of endplates for rapsyn–EGFP (left-hand panels) and corresponding TRITC-α-BGT fluorescence (right-hand panels) demonstrates specific targeting of rapsyn–EGFP to the endplate, and the absence of significant fluorescent cross-bleed. Muscle fibres were electroporated with rapsyn–EGFP (*A*, *B*, *E* and *F*), EGFP (*C* and *D*) or nothing (*G* and *H*), followed by labelling of endplate AChRs with TRITC-α-BGT (*A–D*, and *G* and *H*). Rapsyn–EGFP targeted to TRITC-α-BGT-labelled endplates (*A* and *B*), while EGFP showed no tendency to target to the endplate (*C* and *D*). Endplates that were not labelled with TRITC-α-BGT showed no significant fluorescence in the TRITC optical channel (*E* and *F*). Similarly, nontransfected endplates showed no detectable fluorescence on the EGFP channel (*G* and *H*). *I*, scatter plot showing the spatial correlation of rapsyn–EGFP and TRITC-α-BGT staining within a single postsynaptic AChR cluster. AChR and rapsyn–EGFP images of the same endplate were pixilated, and each pixel was plotted for TRITC intensity *versus* EGFP intensity on scatter plots (see Methods). This revealed a close linear correlation between the fluorescence intensity of TRITC-α-BGT-labelled AChRs and rapsyn–EGFP (diagonal line). Negative controls consisting of fibres that were not labelled with TRITC-α-BGT or not transfected with rapsyn–EGFP (vertical and horizontal lines, respectively) showed no correlation of fluorescence levels between images captured using EGFP and TRITC channels. *A–H*, scale bar, 10 μm.

endplate was then normalized to TRITC-α-BGT intensity so as to measure the accumulation of rapsyn–EGFP at endplates (Fig. 6*B*). This revealed two things. Firstly, throughout days 1–11 after electroporation, the ratio of rapsyn–EGFP to AChR varied substantially from endplate to endplate. Presumably variations between fibres in the level of expression of rapsyn–EGFP resulted in variable occupancy of the available rapsyn binding sites. Secondly, the average rapsyn–EGFP to AChR fluorescence ratio reached a plateau level of about 0.8 by 1 day after electroporation, and this was maintained through to 11 days (the last time point examined; Fig. 6*B*). This suggests that there are a limited number of extra-binding sites (per AChR) for rapsyn to occupy. These results certainly do not rule out the possibility that rapsyn–EGFP assembled with AChR in the Golgi apparatus. They do provide clear evidence that rapsyn–EGFP can target rapidly to limited number of extra-binding sites at the endplate, presumably by binding directly to the pre-existing postsynaptic AChR cluster.

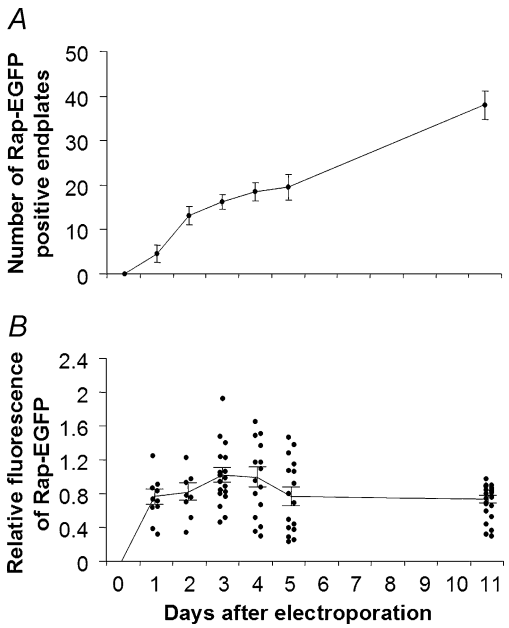

Figure 6. Changes in the number of rapsyn–EGFP-positive endplates and the fluorescence intensities of endplates
A, following electroporation with rapsyn–EGFP, the number of endplates per TA muscle that displayed rapsyn–EGFP fluorescence increased at a fairly steady rate from 1 to 11 days after electroporation. *B*, the mean rapsyn–EGFP fluorescence intensity of individual endplates was normalized to the fluorescence of TRITC-α-BGT. Within 1 day after electroporation, the mean intensity of rapsyn–EGFP fluorescence had reached a value in the steady-state range of about 80% of TRITC-α-BGT intensity. Individual endplates varied considerably in the ratio of rapsyn–EGFP to TRITC-α-BGT intensity, presumably due to variation in the level of rapsyn–EGFP expression among fibres. Data in *A* represent the mean ± S.E.M. for 5 mice at each age point. Data points in *B* are individual endplates (curve fitted to mean and S.E.M.).

Rapsyn–EGFP occupies previously unpopulated rapsyn binding sites at endplates

Two antirapsyn monoclonal antibodies, mAb1234 and mAb1579 (Froehner, 1984), recognize N- and C-terminal epitopes in rapsyn, respectively. Both antibodies recognized wild-type rapsyn equally well by immunofluorescence, but mAb1579-labelled rapsyn–EGFP only weakly, presumably due to steric hindrance by the C-terminal EGFP moiety (see supplementary information). The two antirapsyn antibodies were used to probe transverse cryosections of muscle containing rapsyn–EGFP-positive endplates, and rapsyn–EGFP-negative (control) endplates on neighbouring fibres within the same sections (Fig. 7*A*). Fluorescence quantification showed that rapsyn–EGFP-positive endplates stained more brightly with mAb1234 compared with rapsyn–EGFP-negative endplates (Fig. 7*B*; $P < 0.001$, $n = 39$). This increase in immunoreactivity for total rapsyn (rapsyn–EGFP + endogenous wild-type rapsyn) suggests that the rapsyn–EGFP bound some additional, previously unoccupied, binding sites at the endplate, thereby increasing the total density of rapsyn at the endplate about 1.8-fold. In contrast, the intensity of mAb1579 staining (selective for wild-type rapsyn) was significantly reduced at rapsyn–EGFP-positive endplates (Fig. 7*B*; $P < 0.05$, $n = 56$). This reduction (~25%) might reflect partial replacement of endogenous (wild-type) rapsyn with rapsyn–EGFP during the 5 days postelectroporation due to ongoing slow turnover of the rapsyn–AChR complex. On the other hand, we cannot fully exclude the possibility that the reduction in mAb1579 staining might be due to a selectively impaired access of mAb1579 IgG to endogenous rapsyn at rapsyn–EGFP-positive endplates. Quantification of TRITC-α-BGT fluorescence indicated that targeting of rapsyn–EGFP to the endplate made no significant difference in the overall density of AChR at these endplates (Fig. 7*B*).

Rapsyn–EGFP can stabilize AChRs at the endplate

We investigated the possibility that increases in the ratio of rapsyn to AChR at the endplate might stabilize AChR, inhibiting normal metabolic turnover. Four days after electroporation of rapsyn–EGFP, mice were anaesthetized and the surface of the muscle was bathed with TRITC-α-BGT to label AChRs. Mice were killed and the TA was frozen either immediately (experimental day 4), or after a further 4 days of running around the cage (experimental day 8). Cryosections transverse to the long axis of the muscle fibres were processed and imaged together. Optical sections of rapsyn–EGFP-positive and -negative endplates were imaged in the same cryosections. Figure 8*A* and *B* shows an example of such a comparison at day 8. Residual TRITC-α-BGT fluorescence was stronger at the rapsyn–EGFP-positive endplate (arrow in Fig. 8*B*) than the rapsyn–EGFP-negative endplate (arrowhead). The mean pixel intensity values for multiple endplates were quantified in Fig. 8*C*–*E*. The presence of rapsyn–EGFP at endplates had no effect upon the intensity of endplate TRITC-α-BGT in muscles frozen at the time of labelling (Fig. 8*C*). However, in mice that were allowed to run around for 4 days (until day 8), TRITC-α-BGT was 26% brighter at rapsyn–EGFP-positive than rapsyn–EGFP-negative endplates (Fig. 8*D*). This indicates that the presence of rapsyn–EGFP slowed the time-dependent loss of AChR from endplates. Sister day 8 sections were re-exposed to TRITC-α-BGT to label total AChR (residual plus newly incorporated; Fig. 8*E*). Once again, rapsyn–EGFP at endplates made no significant

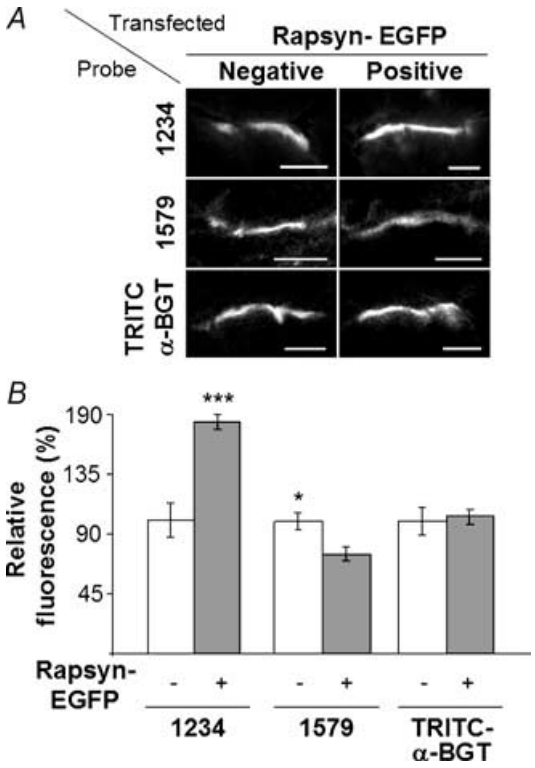

Figure 7. Rapsyn–EGFP occupied spare rapsyn binding sites at the endplate
A, transverse cryosections of endplates on TA muscle fibres transfected with rapsyn–EGFP were immunolabelled with either monoclonal antibody (mAb)1234 (top), mAb1579 (middle) or TRITC-α-BGT (bottom). Rapsyn–EGFP-positive endplates and -negative (control) endplates are shown. *B*, quantification of the fluorescence intensity showed increased levels of mAb1234 antirapsyn staining at rapsyn–EGFP-positive endplates, indicating that total rapsyn was increased at these endplates compared with rapsyn–EGFP-negative fibres (***$P < 0.001$). Antirapsyn mAb1579 staining was significantly reduced at rapsyn–EGFP-positive endplates compared to the rapsyn–EGFP-negative fibres (*$P < 0.05$). The intensity of TRITC-α-BGT-labelled AChRs was not significantly different between rapsyn–EGFP-positive and -negative endplates. Data represent the mean ± S.E.M. for a minimum of 10 endplates in each instance. For each pair of bars in *B*, fluorescence was normalized to the brightness of the rapsyn–EGFP-negative endplates. *A*, scale bar, 10 μm.

difference in the intensity of total AChR staining. In order to confirm that rapsyn–EGFP could stabilize the AChR at the endplate, we undertook a slightly different experiment. Endplates on the surface of the muscle were electroporated with rapsyn–EGFP then labelled with TRITC-α-BGT 4 days later, as previously described. At day 8, the surface of the intact muscle was imaged to reveal residual AChRs at rapsyn–EGFP-positive and -negative endplates (Fig. 9*A* and *C*). The muscle fibres were then re-exposed to TRITC-α-BGT and the same endplates were imaged again to reveal total AChR (residual plus new added AChR; Fig. 9*B* and *D*). Quantification confirmed that rapsyn–EGFP-positive endplates had significantly brighter residual AChR fluorescence compared with rapsyn–EGFP-negative control endplates (Fig. 9*E*). Furthermore, there was a corresponding reduction in the addition of new receptors to rapsyn–EGFP positive endplates (Fig. 9*E*). Taken together, these results suggest that the targeting of rapsyn–EGFP to the endplate slowed the metabolic turnover of AChR at the adult neuromuscular synapse.

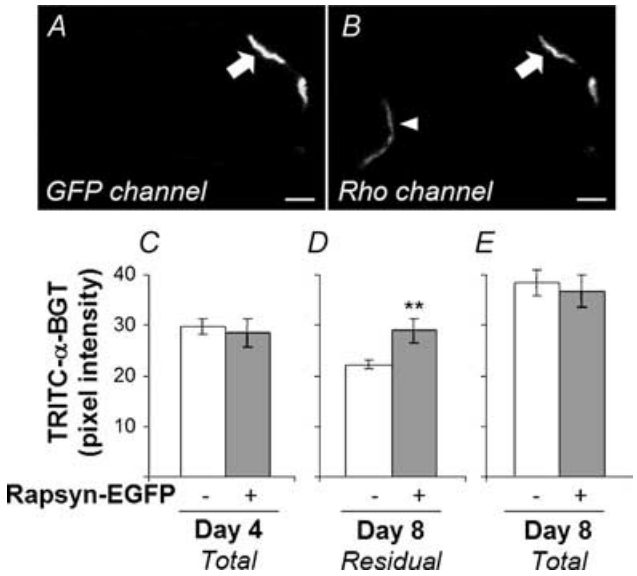

Figure 8. Rapsyn–EGFP inhibited the loss of AChR from the postsynaptic AChR cluster
TA muscles were electroporated with rapsyn–EGFP at day 0. Four days later, AChRs were labelled with TRITC-α-BGT. Transverse cryosections of muscles from mice killed immediately after labelling (Day 4) or 4 days later (Day 8) were processed and imaged together. The brightness of TRITC-α-BGT labelling was compared between rapsyn–EGFP-positive endplates and rapsyn–EGFP-negative endplates within the same cryosections. *A* and *B*, confocal image of a cryosection at day 8. Rapsyn–EGFP-positive (arrow) and -negative (arrowhead) endplates shown in both GFP and rhodamine (TRITC) fluorescence channels (*A* and *B*, respectively). *C*–*E*, quantification of endplate TRITC-α-BGT fluorescence. *C*, there was no difference in endplate TRITC-α-BGT intensity in muscles frozen at the time of labelling (rapsyn–EGFP-negative endplates, $n = 44$; -positive endplates, $n = 10$). *D*, in muscles frozen 4 days later (Day 8), rapsyn–EGFP-negative endplates ($n = 88$) showed a significantly lower TRITC-α-BGT intensity compared with rapsyn–EGFP-positive endplates ($n = 20$; $^{**}P < 0.01$). *E*, sister sections that were re-incubated with TRITC-α-BGT to label total AChR (residual plus new) showed that the presence of rapsyn–EGFP at endplates made no significant difference in the intensity of labelling for total AChR ($n = 23$ and $n = 11$ for rapsyn–EGFP-negative and -positive endplates, respectively). A low gain setting was used in this experiment to avoid pixel saturation. Background fluorescence was measured and subtracted from each endplate. Background fluorescence was always between 10 and 15% of the absolute intensity for the endplate. Scale bar, 10 μm.

Discussion

Much is now known from cell culture and knockout mice about the role of rapsyn in the early development of AChR clusters. However, the adult postsynaptic membrane

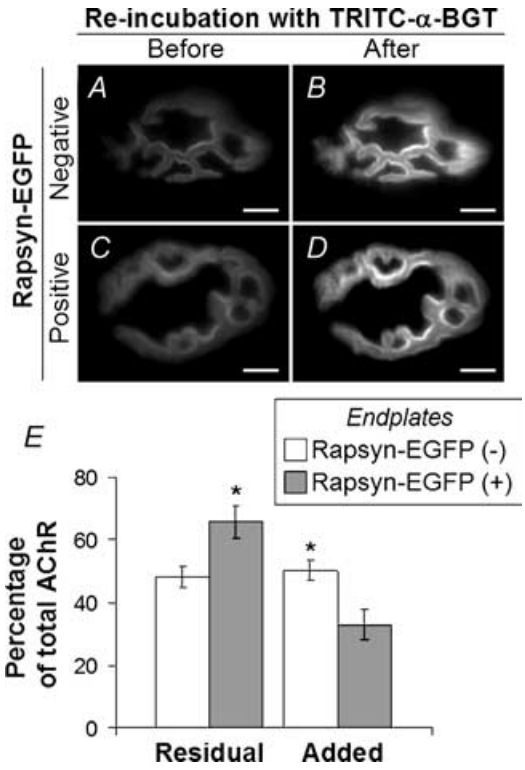

Figure 9. Loss and replacement of AChRs from endplates
Four days after electroporation of rapsyn–EGFP plasmid, the surface of the TA muscle was again exposed, and AChRs were saturated with TRITC-α-BGT. *A* and *C*, on day 8 after electroporation (4 days after TRITC-α-BGT incubation), endplates negative (*A*) and positive (*C*) for rapsyn–EGFP were imaged to reveal AChRs retained from the time of TRITC-α-BGT-labelling 4 days earlier (Residual AChR). The same endplates were imaged again after re-labelling with TRITC-α-BGT to reveal total AChR (*B* and *D*). *E*, quantitative analysis of TRITC-α-BGT fluorescence at endplates (as shown in *A*–*D*). Residual AChR and added AChR (additional AChR revealed by re-labelling with TRITC-α-BGT) were normalized to total TRITC-α-BGT intensity. Rapsyn–EGFP-positive endplates showed higher levels of residual AChR and lower levels of replacement (Added) AChRs compared with rapsyn–EGFP-negative endplates ($^{*}P < 0.05$; $n = 7$ for each group). Scale bar, 10 μm.

is highly specialized compared with embryonic AChR clusters (Sanes & Lichtman, 2001). For example, AChR are packed at a 10-fold higher density and the metabolic half-life of the individual AChRs is 10-fold longer than for AChR clusters in cell culture (Reiness & Weinberg, 1981; Salpeter *et al.* 1986). To begin to understand the role of rapsyn in homeostasis at the mature synapse, we have introduced rapsyn–EGFP into adult muscle fibres. When expressed in extrasynaptic parts of muscle fibres, rapsyn–EGFP targeted to populations of small puncta that colocalized with Golgi markers. Rapsyn–EGFP also targeted directly to the postsynaptic AChR cluster. FRAP experiments showed that rapsyn–EGFP was relatively immobile in both these structures. Quantitative immunohistochemistry indicated that rapsyn–EGFP occupied additional (previously unoccupied) rapsyn binding sites at the endplate. Occupation of these sites slowed the normal metabolic turnover of TRITC-α-BGT-labelled AChR from the postsynaptic AChR cluster. Rapsyn may target to membranes of the exocytic pathway. A substantial fraction of rapsyn–EGFP puncta colocalized with Golgi markers (p115, GM130 and $\alpha-2,6$-sialyltransferase) in pair-wise, double-labelling experiments. The vesicle docking protein p115 and its receptor GM130 are normally associated with the *cis*-Golgi cisternae (Barr & Short, 2003). In contrast, sialyltransferase is a resident of the *trans*-Golgi network (TGN) and, to a lesser extent, the *trans*-Golgi cisternae (Chege & Pfeffer, 1990; Rabouille *et al.* 1995). Our results are consistent with studies of cultured nonmuscle cells showing that rapsyn and AChRs are cotargeted to the plasma membrane via post-Golgi transport vesicles (Marchand *et al.* 2002). The targeting of rapsyn–EGFP to these structures was apparently independent of AChR, since AChRs are not normally expressed in the extrasynaptic regions of muscle fibres. There was also a substantial fraction of rapsyn–EGFP-positive puncta that did not colocalize with Golgi marker (Fig. 4*J*). At present we are not able to account for these. Since we only compared rapsyn–EGFP puncta with one marker at a time, we may have underestimated the degree of colocalization with the Golgi apparatus as a whole. Interestingly, the exocytic pathway may not be the only means of targeting rapsyn to the postsynaptic membrane.

Rapsyn can target to the synapse in two ways: indirectly, by assembling with newly synthesized AChR in the exocytic pathway (as discussed above), and also by directly binding to the cytoplasmic face of the established AChR cluster. Assembly with AChR in the Golgi may well be essential for the formation of the AChR cluster. Agrin-induced AChR clustering does not occur in rapsyn-null muscle cells (Gautam *et al.* 1995; Han *et al.* 1999), nor can rapsyn assemble beneath the postsynaptic nerve terminal in the absence of AChR (Marangi *et al.* 2001; Ono *et al.* 2001, 2004). Presumably, this indirect mode of targeting continues throughout life. Our time course data support the idea that rapsyn can also target directly to the endplate in adult mice. If rapsyn–EGFP is only able to accumulate at the endplate via the ongoing replacement of AChR–rapsyn complex, then we would expect a progressive increase in the relative intensity of rapsyn–EGFP fluorescence at endplates. The half-time to maximal fluorescence would be equivalent to the previously described half-life for turnover of AChR at the adult synapse ($t_{1/2} \approx 10$ days, Salpeter *et al.* 1986; Akaaboune *et al.* 2002). Instead, the mean intensity of rapsyn–EGFP (normalized to TRITC-α-BGT staining), rose abruptly to a plateau within 1 day after electroporation (Fig. 6*B*). We have seen evidence of diffuse, cytosolic rapsyn–EGFP in some electroporated muscle fibres (not shown). Similarly, during the development of the Torpedo electric organ, a substantial fraction of rapsyn within the postsynaptic cell was soluble within the cytosol (Nghiem *et al.* 1991). Thus, it seems likely that rapsyn can rapidly target to available binding sites at the endplate by diffusing through the cytosol. The occupancy of the endplate binding sites might depend upon the level of expression of rapsyn within the cytosol, and possibly also post-translational modifications.

Rapsyn may play an important role in AChR stability. Co-expression of rapsyn with the AChR in cultured muscle and nonmuscle cells produced a significant slowing in the turnover of AChR (maximum $t_{1/2} = 27$ h; Phillips *et al.* 1997; Wang *et al.* 1999). The mechanism for this modest stabilization in cultured cells remains unclear. Nor is it clear how rapsyn might contribute to the dramatic activity- and agrin-dependent postnatal stabilization of AChR (mature $t_{1/2} = 10$ days; Andreose *et al.* 1993; Akaaboune *et al.* 1999; Bezakova *et al.* 2001). Our results indicate that when rapsyn–EGFP occupied extra rapsyn binding sites within the young adult postsynaptic AChR cluster, the normal metabolic turnover of AChRs at the postsynaptic membrane was further slowed. Thus, an increased ratio of rapsyn to AChR may further stabilize endplate AChR without any apparent change in the AChR packing density. In rats, the rapsyn to AChR ratio increases with ageing (Hoedemaekers *et al.* 1998). This might explain why aged rats are resistant to anti-AChR antibody induced receptor loss (De Baets *et al.* 2003). During AChR cluster formation, rapsyn is thought to immobilize AChRs by tethering them to the cytoskeleton (Mohamed & Swope, 1999; Moransard *et al.* 2003), possibly via β-dystroglycan (Cartaud *et al.* 1998; Bartoli *et al.* 2001). Our results are consistent with a model in which rapsyn tethers AChR to a pre-existing submembrane matrix at the adult synapse. We propose that increased stoichiometry of rapsyn to AChR reinforces AChR tethering, thus favouring retention of AChR within the AChR cluster. If so, then physiological changes in the cytosolic concentration of rapsyn, or in rapsyn's avidity for the endplate, might underlie changes in AChR half-life at the synapse.

References

Akaaboune M, Culican SM, Turney SG & Lichtman JW (1999). Rapid and reversible effects of activity on acetylcholine receptor density at the neuromuscular junction *in vivo*. *Science* **286**, 503–507.

Akaaboune M, Grady RM, Turney S & Sanes Lichtman JW (2002). Neurotransmitter receptor dynamics studied *in vivo* by reversible photo-unbinding of fluorescent ligands. *Neuron* **34**, 865–876.

Andreose JS, Xu R, Lomo T, Salpeter MM & Fumagalli G (1993). Degradation of two AChR populations at rat neuromuscular junctions: regulation *in vivo* by electrical stimulation. *J Neurosci* **13**, 3433–3438.

Apel ED, Glass DJ, Moscoso LM, Yancopoulos GD & Sanes JR (1997). Rapsyn is required for MuSK signaling and recruits synaptic components to a MuSK-containing scaffold. *Neuron* **18**, 623–635.

Barr FA & Short B (2003). Golgins in the structure and dynamics of the Golgi apparatus. *Curr Opin Cell Biol* **15**, 405–413.

Bartoli M, Ramarao MK & Cohen JB (2001). Interactions of the rapsyn RING-H2 domain with dystroglycan. *J Biol Chem* **276**, 24911–24917.

Bezakova G, Rabben I, Sefland I, Fumagalli G & Lomo T (2001). Neural agrin controls acetylcholine receptor stability in skeletal muscle fibres. *Proc Natl Acad Sci U S A* **98**, 9924–9929.

Bezakova G & Ruegg MA (2003). New insights into the roles of agrin. *Nat Rev Mol Cell Biol* **4**, 295–308.

Burden SJ, DePalma RL & Gottesman GS (1983). Crosslinking of proteins in acetylcholine receptor-rich membrane: association between the β-subunit and the 43 kDa subsynaptic protein. *Cell* **35**, 687–692.

Cartaud A, Coutant S, Petrucci TC & Cartaud J (1998). Evidence for *in situ* and *in vitro* association between β-dystroglycan and the subsynaptic 43 kDa rapsyn protein. *J Biol Chem* **273**, 11321–11326.

Chege NW & Pfeffer SR (1990). Compartmentation of the Golgi complex: brefeldin-A distinguishes *trans*-Golgi cisternae from the *trans*-Golgi network. *J Cell Biol* **111**, 893–899.

De Baets M, Stassen M, Losen M, Zhang X & Machiels B (2003). Immunoregulation in experimental autoimmune myasthenia gravis- about T-cells, antibodies and endplates. *Ann NY Acad Sci* **998**, 308–317.

Dubinsky JM, Loftus DJ, Fischbach JD & Elson EL (1989). Formation of acetylcholine receptor clusters in chick myotubes: migration or new insertion? *J Cell Biol* **109**, 1733–1743.

Froehner SC (1984). Peripheral proteins of postsynaptic membranes from Torpedo electric organ identified with monoclonal antibodies. *J Cell Biol* **99**, 88–96.

Gautam M, Noakes PG, Moscoso L, Rupp F, Scheller RH, Merlie JP & Sanes JR (1996). Defective neuromuscular synaptogenesis in agrin-deficient mutant mice. *Cell* **85**, 525–535.

Gautam M, Noakes PG, Mudd J, Nichol M, Chu GC, Sanes JR & Merlie JP (1995). Failure of postsynaptic specialization to develop at neuromuscular junctions of rapsyn deficient mice. *Nature* **377**, 232–236.

Glass DJ, Bowen DC, Stitt TN, Radiejewski C, Brunno J, Ryan TE, Gies DR, Shah S, Mattsson K, Burden SJ, DiStefano PS, Valenzuela DM, DeChiara TM & Yancopoulos GD (1996). Agrin acts via a MuSK receptor complex. *Cell* **85**, 513–523.

Godfrey EW & Schwarte RC (2003). The role of nitric oxide signaling in the formation of the neuromuscular junction. *J Neurocytol* **32**, 591–602.

Grady RM, Akaaboune M, Cohen AL, Maimone MM, Lichtman JW & Sanes JR (2003). Tyrosine-phosphorylated and non-phosphorylated isoforms of α-dystrobrevin: roles in skeletal muscle and its neuromuscular and myotendinous junctions. *J Cell Biol* **160**, 741–752.

Han H, Noakes PG & Phillips WD (1999). Overexpression of rapsyn inhibits agrin-induced acetylcholine receptor clustering in muscle cells. *J Neurocytol* **28**, 763–775.

Hoedemaekers A, Bessereau J-L, Graus Y, Guyon T, Changeux J-P, Berrih-Aknin S, van Breda Vriesman P & De Baets M (1998). Role of the target organ in determining susceptibility to experimental autoimmune myasthenia gravis. *J Neuroimmunol* **89**, 131–141.

Huebsch KA & Maimone MM (2003). Rapsyn-mediated clustering of acetylcholine receptor subunits requires the major cytoplasmic loop of the receptor subunits. *J Neurobiol* **54**, 486–501.

LaRochelle WJ & Froehner SC (1986). Determination of the tissue distributions and relative concentrations of the postsynaptic 43-kDa protein and the acetylcholine receptor in Torpedo. *J Biol Chem* **261**, 5270–5274.

Lee MJ, Cho SS, Jang HS, Lim YS, You JR, Park J, Suh H, Kim JA, Park JS & Kim DK (2002). Optimal salt concentration of vehicle for plasmid DNA enhances gene transfer mediated by electroporation. *Exp Mol Med* **34**, 265–272.

Liang SX, Motin L, Moussa CEH, Lavidis NA & Phillips WD (2001). Spatial distribution and developmental appearance of postjunctional P2X1 receptors on smooth muscle cells of the mouse vas deferens. *Synapse* **42**, 1–11.

Marangi PA, Forsayeth JR, Mittaud P, Erb-Vogtli S, Blake DJ, Moransard M, Sander A & Fuhrer C (2001). Acetylcholine receptors are required for agrin-induced clustering of postsynaptic proteins. *EMBO J* **20**, 7060–7073.

Marchand S, Devillers-Thiery A, Pons S, Changeux J-P & Cartaud J (2002). Rapsyn escorts the nicotinic acetylcholine receptor along the exocytic pathway via association with lipid rafts. *J Cell Biol* **22**, 8891–8901.

Megeath LJ, Kirber MT, Hopf C, Hoch W & Fallon JR (2003). Calcium-dependent maintenance of agrin-induced postsynaptic specializations. *Neuroscience* **122**, 659–668.

Mir LM, Bureau MF, Gehl J, Rangara R, Rouy D, Caillaud JM, Delaere P, Branellec D, Schwartz B & Scherman D (1999). High-efficiency gene transfer into skeletal muscle mediated by electric pulses. *Proc Natl Acad Sci U S A* **96**, 4262–4267.

Mittaud P, Marangi PA, Erb-Vogtli S & Fuhrer C (2001). Agrin-activation of acetylcholine receptor-bound src family kinases requires rapsyn and correlates with acetylcholine receptor clustering. *J Biol Chem* **276**, 14505–14513.

Miyazawa A, Fujiyoshi Y, Stowell M & Unwin N (1999). Nicotinic acetylcholine receptor at 4.6Å resolution: transverse tunnels in the channel wall. *J Mol Biol* **288,** 765–786.

Mohamed AS, Rivas-Plata KA, Kraas JR, Saleh SM & Swope SL (2001). Src-class kinases act within the agrin/MuSK pathway to regulate acetylcholine receptor phosphorylation, cytoskeletal anchoring, and clustering. *J Neurosci* **21**, 3806–3818.

Mohamed AS & Swope SL (1999). Phosphorylation and cytoskeletal anchoring of the acetylcholine receptor by src class protein tyrosine kinases: activation by rapsyn. *J Biol Chem* **274**, 20529–20539.

Moransard M, Borges LS, Willmann R, Marangi PA, Brenner HR, Ferns MJ & Fuhrer C (2003). Agrin regulates rapsyn interaction with surface AChRs which underlies cytoskeletal anchoring and clustering. *J Biol Chem* **278**, 7350–7359.

Nghiem HO, Hill J & Changeux JP (1991). Developmental changes in the subcellular distribution of the 43K (n1) polypeptides in Torpedo marmorata electrocyte: support for a role in acetylcholine receptor stabilization. *Development* **113**, 1059–1067.

Ono F, Higashijima S, Shcherbatko A, Fetcho JR & Brehm P (2001). Paralytic zebrafish lacking acetylcholine receptors fail to localize rapsyn clusters to the synapse. *J Neurosci* **21**, 5439–5448.

Ono F, Mandel G & Brehm P (2004). Acetylcholine receptors direct rapsyn clusters to the neuromuscular synapse in zebrafish. *J Neurosci* **24**, 5475–5481.

Phillips WD, Maimone M & Merlie JP (1991). Mutagenesis of the 43-kD postsynaptic protein defines domains involved in plasma membrane targeting and AChR clustering. *J Cell Biol* **115**, 1713–1723.

Phillips WD, Vladeta D, Han H & Noakes PG (1997). Rapsyn and agrin slow the metabolic degradation of the acetylcholine receptor. *Mol Cell Neurosci* **10**, 16–26.

Rabouille C, Hui N, Hunte F, Kieckbusch R, Berger EG, Warren G & Nilsson T (1995). Mapping the distribution of Golgi enzymes involved in the construction of complex oligosaccharides. *J Cell Sci* **108**, 1617–1627.

Ralston E, Ploug T, Kalhovde J & Lomo T (2001). Golgi complex, endoplasmic reticulum exit sites, and microtubules in skeletal muscle fibres are organized by patterned activity. *J Neurosci* **21**, 875–883.

Ramarao MK, Bianchetta MJ, Lanken J & Cohen JB (2001). Role of rapsyn tetratrico repeat and coiled-coil domains in self association and nicotinic acetylcholine receptor clustering. *J Biol Chem* **276**, 7475–7483.

Reiness CG & Weinberg CB (1981). Metabolic stabilization of acetylcholine receptors at newly formed neuromuscular junctions in rat. *Dev Biol* **84**, 247–254.

Salpeter MM, Cooper DL & Levitt-Gilmour T (1986). Degradation rates of acetylcholine receptors can be modified in the postjunctional plasma membrane of the vertebrate neuromuscular junction. *J Cell Biol* **103**, 1399–1403.

Sanes JR & Lichtman JW (2001). Induction, assembly, maturation and maintenance of a postsynaptic apparatus. *Nat Rev Neurosci* **2**, 791–805.

Wang ZZ, Mathias A, Gautam M & Hall ZW (1999). Metabolic stabilization of muscle nicotinic acetylcholine receptor by rapsyn. *J Neurosci* **19**, 1998–2007.

Acknowledgements

We wish to thank Ellie Kable (University of Sydney Electron Microscope Unit) for help with confocal experiments, Dr Kristian Gundersen and Jo Bruusgaard for instruction in muscle electroporation, Anne Turnbull, Nira Chiniah and Jennifer Brockhausen for technical support, and Dr Peter Noakes and Shyuan Ngo for critical reading of the manuscript. This project was supported, in part, by a project grant from the NH & MRC (Australia) and by a Sesqu R & D grant to W.D.P.

Supplementary material

The online version of this paper can be accessed at:
DOI: 10.1113/jphysiol.2004.077685
http://jp.physoc.org/cgi/content/full/jphysiol.2004.077685/DC1
and contains a figure and legend comparing the specificity of the antirapsyn monoclonal antibodies for wild-type rapsyn *versus* rapsyn–EGFP by immunofluorescence.
This material can also be found at:
http://www.blackwellpublishing.com/products/journals/suppmat/tjp/tjp675/tjp675sm.htm